

# Photo-evaporation by thermal winds in dwarf galaxies

Nir J. Shaviv & Avishai Dekel

*Racah Institute of Physics, The Hebrew University, Jerusalem 91904, Israel*

3 November 2018

## ABSTRACT

We revisit the evaporation process of gas from dwarf galaxies after it has been photo-ionized by the UV flux from the first stars and AGNs and heated to  $T \simeq 10^4$  or  $2 \times 10^4$  K respectively. Earlier estimates, based on the balance between pressure and gravity, indicated that dark haloes of virial velocity lower than  $V_{\text{evap}} \simeq 11 - 13 \text{ km s}^{-1}$  have lost most of their gas in a dynamical time. We follow the continuous evaporation by a thermal wind during the period when the ionizing flux was effective. We find that the critical virial velocity for significant evaporation is significantly higher. For example, if the ionization starts at  $z_{\text{ion}} = 10$  and is maintained until  $z = 2$ , a mass loss of one  $e$ -fold occurs in haloes of  $V_{\text{evap}} \simeq 25$  (or  $35 \text{ km s}^{-1}$ ) for  $T \simeq 10^4$  K (or  $2 \times 10^4$  K). Haloes of  $V_{\text{evap}} \simeq 21 \text{ km s}^{-1}$  (or  $29 \text{ km s}^{-1}$ ) lose one  $e$ -fold within the first Hubble time at  $z = 10$ . Any dwarf galaxies with virial velocities smaller than  $V_{\text{evap}}$  must have formed their stars from a small fraction of their gas before  $z_{\text{ion}}$ , and then lost the rest of the gas by photo-evaporation. This may explain the gas-poor, low surface brightness dwarf spheroidal galaxies. By  $z < 1$ , most of the IGM gas was evaporated at least once from dwarf galaxies, thus providing a lower bound to its metallicity.

**Key words:** galaxies: dwarf — galaxies: formation — galaxies: ISM — galaxies: local group — hydrodynamics — winds, outflows

## 1 INTRODUCTION

The first stars and AGNs generate a flux of UV radiation which photoionizes most of the hydrogen in the universe by  $z_{\text{ion}} \sim 7$  (see a review by Barkana & Loeb 2001). The gas is heated to a temperature of  $T_{\text{ion}} \simeq 10^4$  K and is kept at this temperature as long as the ionizing flux persists. The actual temperature mostly depends on the hardness of the radiation flux and therefore on whether its origin is in stars or AGNs, respectively, but also on the flux itself. The total emissivity of the observed quasars at  $z = 3$  is probably sufficient to have completely reionized the low density intergalactic Helium already before that redshift, thereby increasing the temperature to  $T_{\text{ion}} \simeq 2 \times 10^4$  K (Miralda-Escude 2000; Barkana & Loeb 2001). Dark-matter haloes with an escape velocity lower than the associated thermal velocity of the ionized gas, on the order of  $10 \text{ km s}^{-1}$ , cannot retain this hot gas — it would photo-evaporate. Barkana & Loeb (1999) have estimated the gas loss based on the balance between pressure and gravity, and obtained that the haloes that lose 50% of their gas in a dynamical time are of a typical virial velocity of  $V_{\text{evap}} \simeq 11 - 13 \text{ km s}^{-1}$ .

Based on this low estimate of the critical velocity for photo-evaporation, one could have concluded that photo-evaporation is not a very important process in galactic history. This is because a similar lower bound on the virial ve-

locity of haloes that can form stars is obtained from simple cooling arguments. The radiative cooling rate, which is very high just above  $10^4$  K due to atomic recombination, becomes extremely low just below  $10^4$  K. The only available cooling agents in this range are  $H_2$  molecules, which are both inefficient and fragile in the presence of even a weak UV flux (Haiman, Rees & Loeb 1996). This implies that haloes of virial velocity below  $\sim 10 \text{ km s}^{-1}$  cannot have their gas cool to form stars independently of the radiative feedback and the associated reionization. Indeed, there is an indication for such a lower bound in the population of Local Group dwarf galaxies (see Woo & Dekel 2003).

Another scale associated with the radiative feedback process is the Jeans scale. Once the IGM is photo-ionized, its pressure shuts off any further gas infall into haloes of virial velocities up to  $\sim 30 \text{ km s}^{-1}$  (see a review of numerical results in Barkana & Loeb 2001, §6.5). Gas could resume falling into small halos after  $z \sim 1 - 2$  when the UV background flux declined sufficiently (Babul & Rees 1992), but only halos of  $V > 20 - 25 \text{ km s}^{-1}$  can form molecular hydrogen by  $z \sim 1$  (Kepner, Babul & Spergel 1997). This is therefore a lower bound for galaxies unless they managed to have their gas fall into virialized haloes before  $z_{\text{ion}}$ .

The observed internal velocities in Local-Group dwarf galaxies indicate that dwarf galaxies with virial velocities in the range  $10 - 30 \text{ km s}^{-1}$  do exist. However, a compari-

arXiv:astro-ph/0305527v1 28 May 2003

son of the galaxy luminosity function at the faint end (with a logarithmic slope close to  $-1$ ) and the halo mass function predicted by the standard  $\Lambda$ CDM cosmological model (with a log slope near  $-2$ ) indicates that some haloes in this range must have remained dark with no stars in them. Another relevant observation is that most of the galaxies in this range are dwarf spheroidals, showing only little gas and current star formation. This calls for a more careful analysis of the fate of the ionized gas in such haloes. Since an effective ionizing flux may persist until  $z \sim 1-2$  (Babul & Rees 1992), the evaporation process is likely to continue for many dynamical times in the form of a continuous thermal wind, and thus end up with more mass loss than estimated by Barkana & Loeb (1999), and correspondingly with a higher critical velocity  $V_{\text{evap}}$  for significant evaporation. This wind is analogous to the Parker wind from the sun, which is responsible for a mass loss of  $10^{-14} M_{\odot}/\text{yr}$  and is well understood (e.g., Lamers & Cassinelli 1999). With a higher  $V_{\text{evap}}$ , the photo-evaporation would become a major player in the formation of dwarf galaxies. In haloes smaller than this critical velocity (but larger than  $\sim 10 \text{ km s}^{-1}$ ), stars can form only before  $z_{\text{ion}}$ , and any left-over gas cannot be retained. This could lead to the formation of gas-poor dwarfs, not unlike the dwarf spheroidals observed in the Local Group, or to completely dark haloes also in the range  $10 < V < V_{\text{evap}}$ . If a significant fraction of the universal gas was able to evaporate from haloes that managed to form stars earlier, then the evaporation process might also have had implications on the metal enrichment of the IGM. We therefore attempt to evaluate the critical virial velocity for evaporation by pursuing a dynamical calculation of the evaporation process.

In §2 we present the basic treatment of thermal winds applicable to non-point like mass distributions. In §3 we apply the wind analysis to cosmological galactic haloes. In §4 we discuss our results.

## 2 WIND ANALYSIS

We wish to compute the mass-loss rate in a steady isothermal thermal wind in a galactic halo. The formulation is inspired by the standard problem of isothermal winds from stellar objects (Parker 1960; Brandt 1970; Lamers & Cassinelli 1999). The difference is largely in the nomenclature. The main mathematical modification that we have to consider is that the haloes are not point like objects, that is, the gravitational force per unit mass is now  $-GM(r)/r^2 \hat{\mathbf{r}}$  with a monotonically increasing  $M(r)$ .

We begin by considering an arbitrary spherical potential  $\phi(r)$ . The gas is assumed to be heated and kept at a constant temperature  $T$ , typically  $\sim 10^4 \text{ K}$ . Barkana & Loeb (1999) calculated the amount of gas that unbinds “instantaneously” as a result of the extra thermal energy. All the leftover gas, which energetically cannot escape, was assumed to settle down in the haloes’ potential well.

Parker (1960) found that even if the gas is energetically bound, a wind can develop. One way of looking at it is that irrespective of how deep the potential well is, an exponentially small fraction of the gas can escape. Without continuous heating, a thermal wind would progressively cool as it expands, the pressure pushing it out would decrease, and the wind would die out. On the other hand, if the gas

can constantly be heated to compensate for the adiabatic cooling, it is easier for the gas to be expelled, and a large flux can be obtained and maintained.

We assume in the following analysis that the wind is kept at a fixed temperature. This follows from the assumption that over the time scale it takes the gas to accelerate out of the potential well, the radiative equilibrium with the ionizing radiation can keep the gas warm. We will check the consistency of our results with this assumption and discuss its meaning in §3.4.

The basic equations are the continuity equation, the Euler equation of motion, and the equation of state of an isothermal gas:

$$\frac{\partial \rho}{\partial t} = -\nabla \cdot (\rho \mathbf{v}), \quad (1)$$

$$\rho \frac{D\mathbf{v}}{Dt} = -\nabla P + \mathbf{f}_{\text{grav}}, \quad (2)$$

$$P = c_s^2 \rho, \quad (3)$$

where  $c_s$  is the isothermal speed of sound. Under the assumption of spherical symmetry, the equations become

$$\dot{\rho} = -\frac{1}{r^2} (r^2 \rho v)', \quad (4)$$

$$\dot{v} + vv' = -c_s^2 \frac{\rho'}{\rho} - \phi', \quad (5)$$

where  $\phi(r)$  is the gravitational potential normalized to 0 at  $r = 0$ :

$$\phi(r) = \int_0^r \frac{GM(r)}{r^2} dr, \quad (6)$$

and where dot and prime denote Eulerian partial derivatives with respect to  $t$  and  $r$  respectively.

We now assume *steady state*, where  $\dot{M}$  is the same at every  $r$ . Writing  $M = \int 4\pi r^2 \rho dr$ , and using continuity, we obtain  $\dot{M} = -4\pi r^2 \rho v$ . Steady state therefore implies  $r^2 \rho v = \text{const.}$ , and then from continuity  $\dot{\rho} = 0$ . It also requires  $\dot{v} = 0$ . The equations then combine to the *wind equation*:

$$\left( v - \frac{c_s^2}{v} \right) v' = -\phi'(r) + \frac{2c_s^2}{r}. \quad (7)$$

Any *steady state* theory with a *transonic* solution, such as a thermal wind, necessarily requires that the transition between the sub-sonic and super-sonic flow will either take place at a shock (which is of no interest for us here) or that the sonic point will coincide with the critical point where the net radial forces vanish. This is because a transonic solution to eq. 7 implies that the left-hand side changes its sign, and therefore the right-hand side has to change sign at the same radius.<sup>1</sup> Thus, the pressure force has to balance the gravitational force at the sonic point.

The *sonic point*  $r_s$  can therefore be obtained from the given potential profile and the given speed of sound by

$$\phi'(r_s) = \frac{2c_s^2}{r_s}. \quad (8)$$

<sup>1</sup> There are some exceptions to this line of arguments, for example when the force is a function of velocity.

Generally, the solution of this equation is expected to be implicit and it should therefore be solved numerically. Nevertheless, one can anticipate a solution of order  $r_s \sim GM/c_s^2$  (where  $M$  is some typical mass within the sonic radius). In other words, the escape velocity from the sonic radius will generally be of the order of the speed of sound.

We next wish to obtain the *velocity profile* of the wind. By integrating the Euler equation over  $r$ , with the steady-state condition  $\dot{v} = 0$ , we obtain

$$\frac{1}{2}v^2(r) + c_s^2 \ln \rho(r) + \phi(r) = \text{const.}, \quad (9)$$

a constant in  $r$ . By integrating the continuity equation, with the steady-state condition  $\dot{\rho} = 0$ , we obtain

$$\ln \rho(r) + 2 \ln r + \ln v(r) = \text{const.} \quad (10)$$

When combined, the two equations yield:

$$\frac{1}{2} \frac{v^2(r)}{c_s^2} - \ln v(r) - 2 \ln r + \frac{\phi(r)}{c_s^2} = \text{const.} \quad (11)$$

The constant is determined by the requirement that  $v = c_s$  at the sonic point. In exponential form, the equation becomes

$$\frac{v(r)}{c_s} \exp\left(-\frac{v^2(r)}{2c_s^2}\right) = \left(\frac{r_s}{r}\right)^2 \exp\left(\frac{\phi(r)}{c_s^2} - \frac{\phi(r_s)}{c_s^2} - \frac{1}{2}\right). \quad (12)$$

This equation relates the velocity profile and the potential profile, where  $r_s$  is obtained from eq. (8).

The *mass loss rate* can now be evaluated by equating its value at the sonic point and at some small intermediate radius  $r_i$  where  $v \ll c_s$ , using the wind velocity profile of eq. (12). We obtain

$$\begin{aligned} \dot{M} &= 4\pi\rho_s r_s^2 c_s = 4\pi\rho_i r_i^2 v_i \\ &= 4\pi\rho_i r_s^2 c_s \exp\left(\frac{\phi(r_i) - \phi(r_s)}{c_s^2} - \frac{1}{2}\right). \end{aligned} \quad (13)$$

The wind solution is not strictly valid at  $r \rightarrow 0$ , but since we chose  $r_i$  such that  $v \ll c_s$ , we can relate  $\rho(r_i)$  to the gas density  $\rho_0$  at  $r = 0$  via the static solution to eqs. 1 through 3,

$$\rho_0 = \rho_i \exp\left(\frac{1}{c_s^2}[\phi(r_i) - \phi(0)]\right). \quad (14)$$

Thus, the mass loss rate is

$$\dot{M} = 4\pi\rho_0 r_s^2 c_s \exp\left(-\frac{1}{c_s^2}[\phi(r_s) - \phi(0)] - \frac{1}{2}\right). \quad (15)$$

The total mass of gas within  $r_s$ , using eq. (14), is approximately

$$M_{gas}(r_s) = 4\pi\rho_0 \int_0^{r_s} r^2 \exp\left(-\frac{1}{c_s^2}[\phi(r) - \phi(0)]\right) dr. \quad (16)$$

The *evaporation time scale*, defined by  $\tau_{evap} \equiv M_{gas}/\dot{M}$ , can now be obtained from eq. (16) and eq. (15):

$$\tau_{evap} = \frac{\sqrt{e}}{c_s} \int_0^{r_s} \left(\frac{r}{r_s}\right)^2 \exp([\phi(r_s) - \phi(r)]/c_s^2) dr. \quad (17)$$

Note that it does not involve the values of the potential or the density at the halo center.

To obtain the above result, we implicitly assumed that the static solution, eq. (14), is valid for the density out to  $r_s$ . This is a sensible approximation as long as the bulk of the mass at  $r < r_s$  has  $v \ll c_s$ . Under this limit, where most of

the mass is almost at rest, the total mass estimate of eq. (16) is valid. If we only have  $v \leq c_s$ , a large fraction of the mass evaporates on an acoustic time scale – the sound crossing time of the characteristic length  $r_s$ . In this case we do not have a steady state and the system should be treated in another limit, as in Barkana & Loeb (1999). Quantitatively, the requirement that our solution be valid is therefore

$$\tau_{evap} \gg \tau_{acoustic} \equiv r_s/c_s. \quad (18)$$

In order to apply the above result, we need a potential profile and the value of  $c_s$  as input. We then find the sonic point by eq. (8), and then use eq. (15) or eq. (17).

### 3 APPLICATION TO REALISTIC HALOES

#### 3.1 An NFW Profile

We apply the above evaporation analysis to the typical profile of galactic haloes, as seen in cosmological N-body simulations of the standard  $\Lambda$ CDM cosmology. The dark-matter density is assumed to follow the NFW profile (Navarro *et al.* 1997):

$$\rho_{dm}(r) = \frac{4\rho_c}{x(1+x)^2}, \quad x \equiv \frac{r}{r_c}, \quad (19)$$

where  $r_c$  is a characteristic inner radius<sup>2</sup> and  $\rho_c$  is the density at  $r_c$ . The mass profile is obtained by an integral over  $r$ :

$$M_{dm}(r) = 16\pi\rho_c r_c^3 A(x), \quad A(x) \equiv \ln(1+x) - \frac{x}{1+x}. \quad (20)$$

We may replace below the parameter  $\rho_c$  by  $M_c$ , the mass enclosed within  $r_c$ , which is given by

$$M_c = 8\pi\rho_c r_c^3 (\ln 4 - 1). \quad (21)$$

Assuming that the gravity is dominated by the dark matter, the gravitational force is

$$f_{grav}(r) = -\frac{GM_{dm}(r)}{r^2} = -16G\pi r_c \rho_c \frac{A(x)}{x^2}, \quad (22)$$

and the potential is:

$$\phi(r) = -\int_0^r f_{grav}(r) dr = 16G\pi r_c^2 B(x) \quad (23)$$

where

$$B(x) \equiv \frac{x - \ln(1+x)}{x}. \quad (24)$$

The sonic point  $r_s$  is the solution of eq. (8), which takes the form:

$$\frac{A(x_s)}{x_s} = \frac{(\ln 4 - 1)}{\psi}, \quad \psi \equiv \frac{GM_c/r_c}{c_s^2}. \quad (25)$$

The dimensionless parameter  $\psi$  characterizes the general behavior of the gas in the given system. It relates the gravitational potential at the core radius to the specific thermal energy of the gas. In other words, it is the ratio squared between the circular velocity at the core radius and the isothermal speed of sound. Depending on the value of  $\psi$ , the system could be in one of the following three regimes.

<sup>2</sup> One may loosely use the term ‘‘core’’ radius even when it is actually a steeper ‘‘cusp’’.

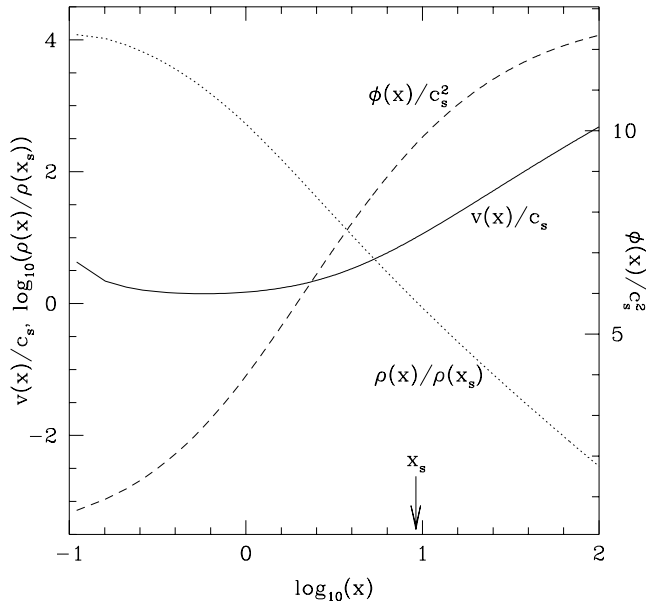


**Figure 1.** The solution for the evaporation of gas from an NFW potential, with  $\psi \equiv (GM_c/r_c)/c_s^2 = 2.5$ , in the regime where the evaporation is through a steady wind. The sonic point is at  $x_s = 9.18$ . Shown are the NFW potential  $\phi(x)$  in units of  $c_s^2$ , the gas velocity in units of  $c_s$ , and the gas density  $\rho(x)$  in units of its value at the sonic point. Note that since the sonic point is likely to be comparable to the virial radius, our spherical solution may become invalid outside the sonic point. This does not change the estimates of the mass loss, but it may change the expected gas velocity at large radii.

A value of  $\psi \gg 1$  implies that the gas is tightly bound and the evaporation is negligible. When  $\psi > 1$  but  $\psi$  is not too large, we expect a steady-state evaporation by a thermal wind over many dynamical time scales. On the other hand, when  $\psi \lesssim 1$ , we expect no steady-state behavior and the gas evaporates rapidly over a few dynamical time scales. By solving eq. (25), we obtain the dimensionless sonic radius  $x_s(\psi)$ .

Once  $x_s$  is found, we can obtain the actual wind solution. To do so, we take the NFW potential, eq. (23), and plug it in eq. (12), which is an implicit equation for  $v(r)/c_s$ . This equation can then be solved numerically. The solution for the wind velocity profile  $v(x)$ , together with the gas density profile  $\rho(x)$  and the NFW potential, are plotted in fig. 1 for the specific case of  $\psi = 2.5$ , for which  $x_s = 9.18$ . An interesting point to note is that this sonic radius is comparable to the virial radius in a typical NFW halo, which is on the order of  $R_v \sim 10r_c$  (see Bullock *et al.* 2001a). This implies that the wind solution at the sonic point may be perturbed by deviations from spherical symmetry due to neighboring haloes. This may have a noticeable effect on the velocity attained by the evaporated gas, but since the sonic point is determined by conditions internal to it, we expect no significant effect on the mass-loss rate itself. This is because, by definition, material past the sonic point is moving too fast to acoustically affect conditions up stream.

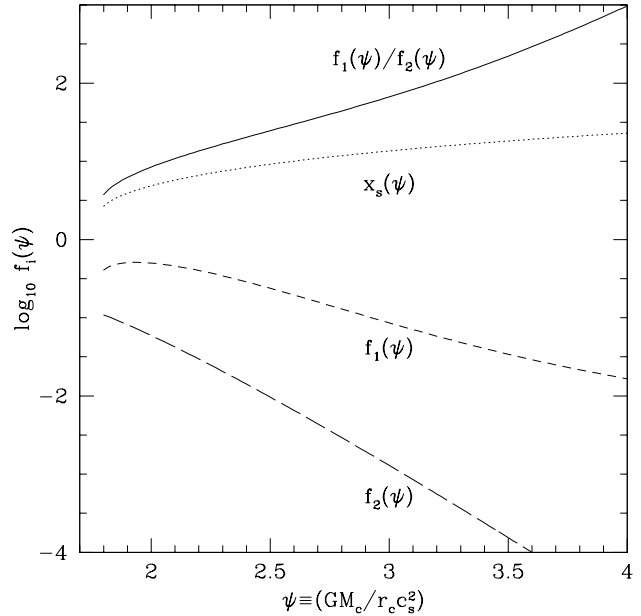


**Figure 2.** The dimensionless functions of  $\psi$  for NFW haloes, where  $\psi$  characterizes the ratio of potential to thermal energy. For  $\psi < 1.78$  there is no steady state solution, and evaporation takes place after a few sound-crossing times. The function  $x_s(\psi)$  is the radius of the sonic point in units of the core radius. The function  $f_1(\psi)$  is the gas mass within the sonic point in units of  $4\pi/3\rho_0r_c^3$  where  $\rho_0$  is the gas density at  $r = 0$ . The function  $f_2(\psi)$  is the mass-loss rate in the above mass units per sound crossing time  $r_c/c_s$ . The ratio  $f_1(\psi)/f_2(\psi)$  is the thermal evaporation time scale in units of  $r_c/c_s$ .

A useful dimensionless function of  $\psi$  is the gas mass within  $r_s$  in units of  $(4\pi/3)\rho_0r_c^3$ :

$$f_1(\psi) \equiv \frac{M_{gas}}{(4\pi/3)\rho_0r_c^3} \quad (26)$$

$$= 3 \int_0^{x_s(\psi)} x^2 \exp\left[-\frac{2\psi}{(\ln 4 - 1)}B(x)\right] dx,$$

where  $M_{gas}$  is taken from eq. (16) with the NFW potential from eq. (23). Note that  $\psi$  enters both in the integrand and through the upper limit of the integration  $x_s(\psi)$ .

Another useful dimensionless function of  $\psi$  is the mass-loss rate in units of  $(4\pi/3)\rho_0r_c^3$  per the gas acoustic time scale  $r_c/c_s$ :

$$f_2(\psi) \equiv \frac{\dot{M}}{(4\pi/3)\rho_0r_c^3/(r_c/c_s)} \quad (27)$$

$$= 3 \exp\left[-\frac{1}{2} - \frac{2\psi}{(\ln 4 - 1)}B[x_s(\psi)]\right].$$

The evaporation time scale, for an  $e$ -fold mass loss, is therefore, as in eq. (17), given by:

$$\tau_{evap} = \frac{M_{gas}}{\dot{M}} = \frac{r_c f_1(\psi)}{c_s f_2(\psi)}. \quad (28)$$

The solution of  $x_s(\psi)$ , together with the functions,  $f_1(\psi)$ ,  $f_2(\psi)$ , and  $f_1(\psi)/f_2(\psi)$ , are depicted in fig. 2, as a function of  $\psi$ . The ratio  $f_1(\psi)/f_2(\psi)$  gives the evaporation

time scale in units of the sound crossing time. Take, for example, the case where  $\psi = 3$ . Most of the gas is dynamically bound, as the potential energy dominates over the thermal energy, but the evaporation process could be important if enough time is available. In this case,  $f_1(\psi)/f_2(\psi) \approx 50$ , such that it takes about 50 sound crossing times of the core radius to evaporate the gas.

### 3.2 Haloes of different mass and velocity

Since we wish to compare the above results to actual cosmological haloes, it is convenient to express the NFW profile parameters in terms of the “virial” quantities: the radius  $R_v$ , the mass interior to it  $M_v$ , and the circular velocity at the virial radius  $V_v$ . Also, instead of using the more physically relevant acoustic time scale, we should express the evaporation time in units of the Hubble time at the corresponding cosmological epoch.

At redshift  $z$ , the virial mass is related to the virial radius through the universal top-hat overdensity  $\Delta$  at virialization:

$$M_v \equiv \frac{4\pi}{3} \Delta(z) \rho_u R_v^3, \quad (29)$$

where  $\rho_u$  is the average universal density at  $z$ . The corresponding virial velocity is defined by

$$V_v^2 \equiv \frac{GM_v}{R_v}. \quad (30)$$

For the family of flat cosmologies ( $\Omega_m + \Omega_\Lambda = 1$ ), the virial overdensity can be approximated (Bryan & Norman 1998) by:

$$\Delta(z) \approx \frac{(18\pi^2 + 82[\Omega_m(z) - 1] - 39[\Omega_m(z) - 1]^2)}{\Omega_m(z)}, \quad (31)$$

where  $\Omega_m(z)$  is the mass density parameter at redshift  $z$ . It is related to today’s values of the cosmological parameters by

$$\Omega_m(z) \approx \frac{\Omega_{m0}(1+z)^3}{\Omega_{m0}(1+z)^3 + 1 - \Omega_{m0}}. \quad (32)$$

At the high redshifts of relevance to us here,  $\Omega_m$  is close to unity, and  $\Delta(z) \approx 180$ . For the standard  $\Lambda$ CDM cosmology, with  $\Omega_{m0} = 0.3$  and  $\Omega_{\Lambda0} = 0.7$ , today’s value is  $\Delta(z=0) \approx 340$ .

If we define a factor of order unity by

$$F_1 \equiv \frac{\Omega_{m0}}{0.3} \frac{\Delta(z)}{200} \left( \frac{h}{0.7} \right)^2, \quad (33)$$

where  $h$  is the Hubble constant in units of  $100 \text{ km s}^{-1} \text{ Mpc}^{-1}$ , we can write the above virial relations (to an accuracy better than 1%) as

$$M_8 = 0.342 F_1 (1+z)^3 R_{10}^3, \quad (34)$$

$$V_{10} = 0.383 F_1^{1/2} (1+z)^{3/2} R_{10}, \quad (35)$$

$$M_8 = 6.06 F_1^{-1/2} (1+z)^{-3/2} V_{10}^3, \quad (36)$$

where  $M_8 \equiv M_v/10^8 M_\odot$ ,  $R_{10} \equiv R_v/10 \text{ kpc}$ , and  $V_{10} \equiv V_v/10 \text{ km s}^{-1}$ .

To relate the virial variables to the core characteristics of the NFW profile we use the concentration parameter, defined by

$$C \equiv R_v/r_c. \quad (37)$$

At a given  $M_v$  and  $z$ , we use here the average concentration parameter as derived by Bullock *et al.* (2001a) from an  $N$ -body simulation of the  $\Lambda$ CDM cosmology. It can be approximated by

$$C(M_v, z) \approx 20 (1+z)^{-1} \left( \frac{M_v}{10^{11} M_\odot} \right)^{-0.13}. \quad (38)$$

Once we combine the above relations to the results obtained for the thermal evaporation of the gas, we are in a position to evaluate the evaporation process of typical cosmological haloes. In particular, we can compare the evaporation time scale, by which the halo has lost an  $e$ -fold of its gas mass, to the Hubble-expansion time scale at the onset of ionization,  $z_{\text{ion}}$ . This is depicted in fig. 3, where we plot  $\tau_{\text{evap}}/\tau_{\text{Hubble}}(z_{\text{ion}})$  for a set of initial and terminal redshifts for the ionizing radiation. From the figure, it is apparent that for earlier values of  $z_{\text{ion}}$ , the thermal evaporation process can evaporate gas from haloes with a somewhat higher virial velocity. This is mainly because at a higher redshift a halo of a given  $V_v$  has a smaller  $\psi$ , roughly  $\psi \propto (1+z)^{-0.8}$ . [It comes about because, for a given  $V_v$ ,  $R_v \propto M_v \propto (1+z)^{-3/2}$  and roughly  $C \propto (1+z)^{-0.8}$ , such that  $r_c \equiv R_v/C \propto (1+z)^{-0.7}$ . On the other hand,  $M_v \propto (1+z)^{-3/2}$ , and  $M_c/M_v$  is only a weak function of  $C$ . Together, with  $c_s$  the same at all redshifts, we get that roughly  $\psi \propto M_c/r_c \propto (1+z)^{-0.8}$ .] We see in Fig. 2 that  $f_1/f_2$  is varying exponentially with  $\psi$ ,  $f_1/f_2 \propto e^{b(1+z)^{-1/2}}$ , so we expect a high reduction in  $f_1/f_2$  at a high  $z$ . The multiplication by  $r_c \propto (1+z)^{-0.7}$  in eq. (28) makes the decrease of  $\tau_{\text{evap}}$  with  $z$  even steeper. The corresponding decrease in  $\tau_{\text{Hubble}}$ , which at early times is  $\propto (1+z)^{-3/2}$ , weakens the decrease of  $\tau_{\text{evap}}/\tau_{\text{Hubble}}$  with  $z$ , but it is not steep enough to compensate for the exponential decrease in  $\tau_{\text{evap}}$ . The net result is therefore an increase in the evaporation efficiency as a function of  $z$ . For example, if  $t = 10^4 \text{ K}$ , the critical velocity for  $e$ -fold loss in one Hubble time grows from  $V_v = 18.8 \text{ km s}^{-1}$  at  $z_{\text{ion}} = 1$  to  $V_v = 22.0 \text{ km s}^{-1}$  at  $z_{\text{ion}} = 20$ . However, if the ionizing flux remains effective until, say,  $z = 1$ , the critical velocity for  $z_{\text{ion}} = 20$  becomes  $V_v = 27.7 \text{ km s}^{-1}$ .

The terminal redshift, when the ionizing radiation is switched off, is also a factor in determining the critical halo virial velocity from which gas can evaporate. For example, if  $T = 10^4 \text{ K}$  and  $z_{\text{ion}} = 10$ , haloes that lose an  $e$ -fold of their gas in either one Hubble time, by  $z = 5$ ,  $z = 2$ , or  $z = 1$ , are of  $V_v \approx 21.5, 22.3, 25.5$ , and  $26.4 \text{ km s}^{-1}$  respectively.

On the other hand, the temperature at which the gas can be kept heated is more important at determining the evaporation losses. This is because it determines the speed of sound. Since  $c_s \propto \sqrt{T}$ , all typical velocities in the system scale in the same manner. Namely, by increasing  $T$  from  $10^4 \text{ K}$  to  $2 \times 10^4 \text{ K}$ , the critical velocity for  $e$ -fold evaporation becomes larger by a factor of  $\sim \sqrt{2}$ . For example, if  $z_{\text{ion}} = 10$ , the critical velocity for an  $e$ -fold loss in a Hubble time grows from  $V_v = 21.5 \text{ km s}^{-1}$  for  $T = 10^4 \text{ K}$  to  $V_v = 29.3$  for  $T = 2 \times 10^4 \text{ K}$ .

The intersections between the acoustic curves and the evaporation curves plotted in fig. 3, correspond to the lowest velocities for which there is a consistent steady state thermal evaporation, and  $e$ -fold mass loss over a dynamical time. These velocities are somewhat larger than the ve-

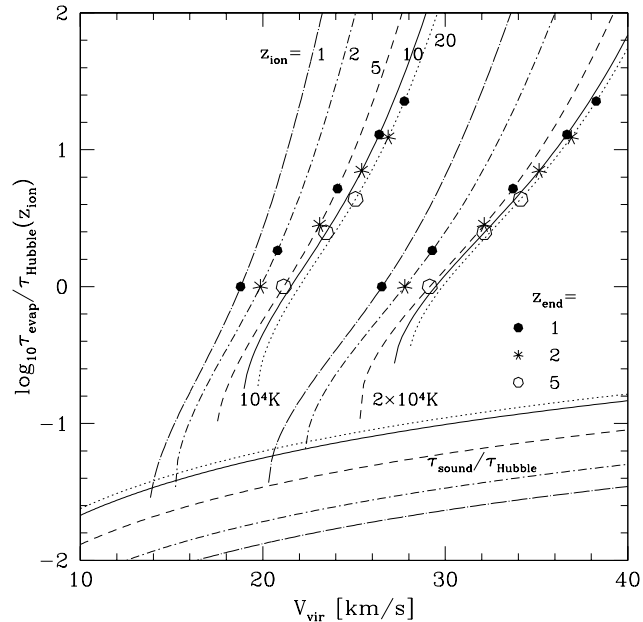


**Figure 3.** The evaporation time of haloes with different virial velocities  $V_v$ . The calculation is carried out at different redshifts  $z_{\text{ion}}$  when the gas is assumed to be photo-ionized (as marked). The evaporation time is expressed in units of the Hubble time at that  $z_{\text{ion}}$ . The sets of curves on the left and on the right correspond to  $T = 10^4\text{K}$  and  $2 \times 10^4\text{K}$  respectively. The velocity at which the curve reaches  $\tau_{\text{evap}}/\tau_{\text{Hubble}} = 1$  marks the critical virial velocity of a halo that loses an  $e$ -fold of its gas in one Hubble time. Also marked on each curve are the Hubble times at later redshifts  $z_{\text{end}}$  at which the ionization terminates. For example, a halo which is ionized at  $10^4\text{K}$  at  $z_{\text{ion}} = 10$  (the solid curve in the left set), and is subject to an effective ionizing flux until  $z_{\text{end}} = 1$  (the dot on the curve), will decrease its gas mass by an  $e$ -fold if its virial velocity is  $V_v = 26.4\text{ km s}^{-1}$ . If  $T = 2 \times 10^4\text{K}$ , a halo of  $V_v = 36.8\text{ km s}^{-1}$  will suffer a similar mass loss by  $z = 1$ . The lower set of curves is the “acoustic time scale” for the different redshifts. Our wind calculation is valid as long as this time scale is much smaller than  $\tau_{\text{evap}}$ .

locities corresponding to instantaneous mass loss found by Barkana & Loeb (1999) using binding energy arguments.

The fraction of gas not evaporated decreases exponentially with time, such that over a given time  $\Delta t$ , this fraction is  $\exp(-\Delta t/\tau_{\text{evap}})$ . Thus, using the evaporation time scale, we can estimate the amount of gas that will evaporate over a Hubble time. This is described in fig. 4, which plots the fraction of evaporated gas as a function of the virial mass of the halo, or the virial velocity in the inset. Also plotted is the fraction of gas which becomes unbound and “instantly” evaporates on a dynamical time scale once ionization is switched on, as calculated by Barkana & Loeb (1999).

From the figure, it is evident that by letting the slow process of thermal evaporation take place, a given relative mass loss is obtained in haloes which are typically 10 times more massive. For example, only haloes of  $\lesssim 2 \times 10^7 M_\odot$  ( $\lesssim 10\text{ km s}^{-1}$ ) lose 70% of their gas mass from the instantaneous evaporation, while the thermal wind ensures that haloes with  $\lesssim 2 \times 10^8 M_\odot$  ( $\lesssim 22\text{ km s}^{-1}$ ) lose 70% of their

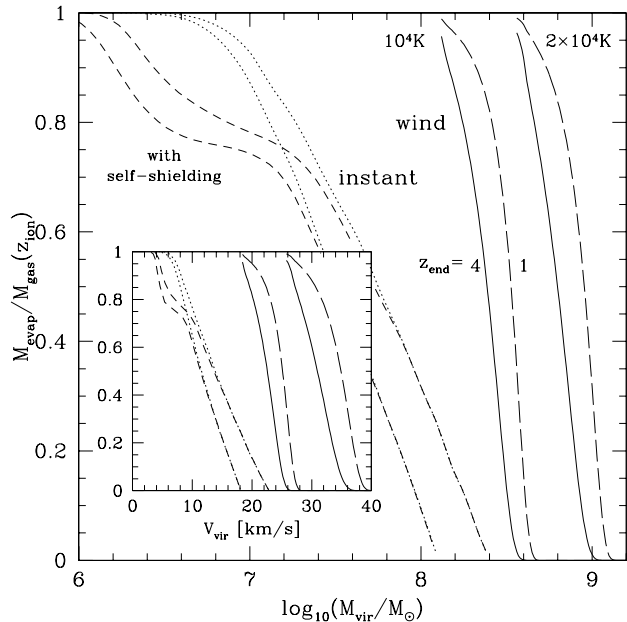


**Figure 4.** Fraction of gas mass evaporated from haloes due to re-ionization at  $z_{\text{ion}} = 8$  as a function of halo mass or virial velocity (inset). The two pairs of curves on the right are the results of evaporation by thermal wind continuing until  $z_{\text{end}} = 4$  and 1, for  $T = 10^4$  and  $2 \times 10^4\text{K}$  as marked. The two pairs of curves on the left are the gas fraction evaporated instantaneously according to Barkana & Loeb (1999). In each pair, the curves are for  $T = 10^4$  (left) and  $2 \times 10^4\text{K}$  (right). The pair of curves on the very left, showing less evaporation at small masses, represents the inclusion of self shielding, which enables the existence of a dense core inaccessible to the effects of the external ionizing radiation. We find that the continuous evaporation by wind increases the critical mass for evaporation by an order of magnitude, and it sharpens the transition between efficient and inefficient evaporation.

gas mass, if  $T = 10^4\text{K}$ . For  $T = 2 \times 10^4\text{K}$ , the equivalent mass increases by more than a factor of two. In the case of haloes which suffered higher mass loss fractions, we find that the inclusion of thermal evaporation can increase the equivalent cutoff virial mass by almost 100-fold. This is because the thermal wind can even evaporate the dense cores which otherwise are shielded from the ionizing radiation and therefore do not evaporate dynamically.

We also see in the figure that the process has a sharp cutoff, that is, either a halo can or it cannot retain its gas. Only a very narrow range of halo masses partially retain their original gas content. Also apparent is that the critical halo mass is not sensitive to the epoch when the ionization becomes ineffective. We learned in Fig. 3 that it is also not too sensitive to the epoch when the ionization starts, but it is quite sensitive to the temperature at the ionized state.

### 3.3 Mass budget

Next, we wish to evaluate the total fraction of gas evaporated from haloes during the ionization period. We consider the distribution of halo masses at  $z_{\text{ion}}$  and integrate over the fraction of gas evaporated from each of these halos, either in-

stantaneously or under the assumption that the ionization remains effective until  $z_{\text{end}} = 2$ . The results are shown in Fig. 5.

The distribution of halo masses is estimated using the Sheth-Tormen modification (Sheth & Tormen 1999) of the Press-Schechter approximation. Assuming a cosmological model and Gaussian initial fluctuations with a given linear power spectrum, the fraction of mass in haloes of virial mass larger than  $M$  is estimated by

$$F(> M, z) = 0.4 \left( 1 + \frac{0.4}{\nu^{0.4}} \right) \text{erfc} \left( \frac{0.85\nu}{\sqrt{2}} \right), \quad (39)$$

where  $\nu \equiv \delta_c/[D(z)\sigma(M)]$ , with  $\delta_c = 1.69$ ,  $D(z)$  the linear fluctuation growth rate, and  $\sigma(M)$  the *rms* amplitude of linear density fluctuations today top-hat smoothed over mass  $M$ . We assume the standard flat  $\Lambda$ CDM cosmology with  $\Omega_{m0} = 0.3$  and  $\Omega_{\Lambda0} = 0.7$ . Following Carroll, Press & Turner (1992), we approximate

$$D(z) \approx \frac{\Omega_{m0}^{4/7} + (3/2)\Omega_{m0}}{\Omega_{m0}} \frac{\Omega_m(z)}{[\Omega_m(z)^{4/7} + (3/2)\Omega_m(z)](1+z)}, \quad (40)$$

with  $\Omega_m(z)$  from eq. (32). The *rms* fluctuation  $\sigma(M)$  is derived in the standard way using a top-hat window and the CDM power spectrum of Bardeen *et al.* (1986) with baryonic density  $\Omega_b = 0.044$ , Hubble constant  $h = 0.7$ , power index  $n = 0.95$  and the amplitude of the power spectrum normalized by  $\sigma_8 = 0.85$  (motivated by the best fits from the CMB observations by the MAP satellite).

In Fig. 5, for every value of  $z_{\text{ion}}$ , the gas is divided into three different populations. Below the shaded area is the gas that either has evaporated from mini-haloes of  $V_v < 10 \text{ km s}^{-1}$  (where the inefficient cooling does not allow any stars to form) or “field gas” that has not been in any virialized halo to begin with. The shaded area refers to the fraction of the gas at  $z_{\text{ion}}$  that will be photo-evaporated by  $z_{\text{end}} = 2$  from haloes of  $V_v > 10 \text{ km s}^{-1}$ . The region above the shaded area is the rest of the gas, bound to massive haloes and not to be photo-evaporated. The evaporated fraction is further divided into gas that escapes on a dynamical time scale at  $z_{\text{ion}}$  versus gas that flows out continuously in a thermal wind until  $z_{\text{end}} = 2$ . The results for the two possible gas temperatures are shown.

We find that quite independently of  $z_{\text{ion}}$ , the amount of gas which collapsed into virialized objects and later evaporated is about 6% if the temperature of the gas was kept at  $\sim 2 \times 10^4 \text{ K}$ , or about 4% if  $T$  was kept at  $\sim 10^4 \text{ K}$ . The instant evaporation involved 1 to 1.5% of the gas. In other words, the photo-evaporation process recycled gas in dwarf galaxies, and it can therefore have implications on the metallicity of the IGM.

### 3.4 The assumption of isothermality

The results thus far described should be considered cautiously until we verify the basic assumption behind the evaporation process — that the gas is kept isothermal during the evaporation process. This implicitly assumes that the typical time scale for gas evaporation is longer than the time it takes the expanding gas to heat and establish equilibrium with the radiation field. If this assumption fails, the gas will expand adiabatically instead and cool rapidly with distance.

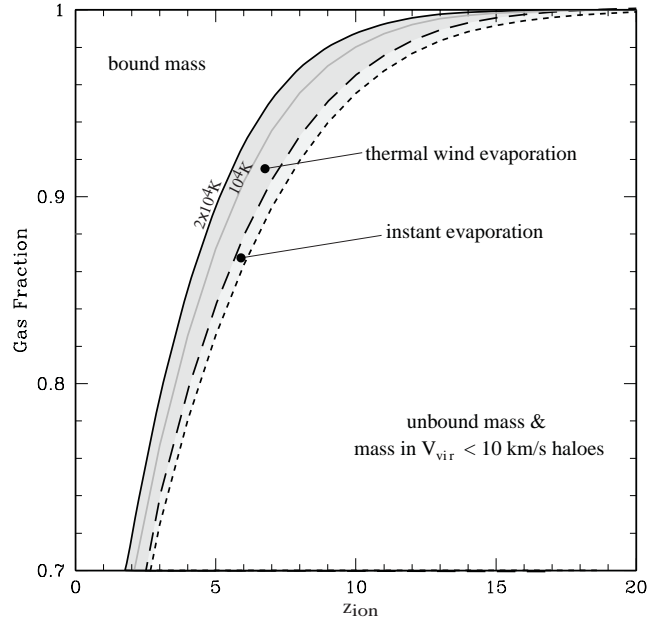


**Figure 5.** “Mass budget” at the onset of reionization  $z_{\text{ion}}$ . The area below the shaded area refers to gas which is either originally associated with haloes of  $V_v < 10 \text{ km s}^{-1}$  or not associated with any virialized halo. This gas is not involved in star-forming galaxies. The gas above the shaded area is bound to massive haloes and it will not photo-evaporate by  $z_{\text{end}} = 2$ . The shaded area refers to the gas that will evaporate from  $V_v > 10 \text{ km s}^{-1}$  haloes. The top two curves refer to continuous evaporation by  $z_{\text{end}} = 2$  for the two possible temperatures as marked. The shaded area between the dashed lines refers to gas that escapes on a dynamical time scale. One may assume that the gas in the shaded strip is recycled in dwarf galaxies and returned to the IGM.

Without the extra energy input from the radiative heating, the net result will be significantly less mass loss from given haloes.

Under the assumption that the ionizing radiation is strong enough to keep the gas hot and in equilibrium between heating and cooling, any additional assumption regarding the heating rate is equivalent to an assumption regarding the cooling rate. Thus, we can test instead the condition that the cooling time is short enough, as compared with the time it takes the gas to outflow from the potential well and reach the sonic point. This is typically the sound crossing time at the virial radius.

From the results of Sutherland & Dopita (1993); Katz, Weinberg & Hernquist (1996), we find that for temperatures in the range  $10^4 \text{ K}$  and  $10^5 \text{ K}$  and for *primordial composition* the cooling rate is  $\Lambda = 5 \times 10^{-23} \Lambda_0 n_H^2 \text{ erg s}^{-1} \text{ cm}^3$ , where  $n_H$  is the number density of the gas and  $\Lambda_0 \approx 1$  to within a factor of two (If the gas is contaminated by metals, the cooling rate could be even faster). The characteristic cooling time can then be defined by  $\tau_{\text{cool}} \equiv (3/2)c_s^2 \rho / \Lambda$ , where  $c_s$  is the *isothermal* speed of sound, corresponding to a temperature  $T$ . The sound crossing time at the virial radius defines the dynamical time,  $\tau_{\text{dyn}} \equiv R_v / c_s$ . We write the gas density as

$\rho = \Delta_b \Omega_b \rho_{crit,0} (1+z)^3$ , where  $\Delta_b$  is the overdensity of baryons at the virial radius, and  $\rho_{crit,0}$  is the critical density of the universe today. Adding these expressions together results with:

$$\frac{\tau_{dyn}}{\tau_{cool}} \approx 1.5 F_2 \left( \frac{V_v}{10 \text{ km s}^{-1}} \right) \left( \frac{\Delta_b}{10} \right) (1+z)^{3/2}, \quad (41)$$

where  $F_2$  is a factor of order unity,

$$F_2 \equiv \left( \frac{\Omega_m \Delta(z)}{0.3 \cdot 200} \right)^{-1/2} \left( \frac{h}{0.7} \right) \left( \frac{\Omega_b}{0.05} \right) \left( \frac{T}{10^4 \text{ K}} \right)^{-3/2} \Lambda_0. \quad (42)$$

In the range of interest we have  $V_v \sim 20 \text{ km s}^{-1}$  and  $z > 1-2$ , so  $\Delta_b > 10$  would guarantee efficient cooling. We can evaluate  $\Delta_b$  in the case where no wind is present by inspecting Fig. 2 of Barkana & Loeb (1999), which shows that  $\Delta_b$  is typically  $\gtrsim 10$ . The presence of a wind can only increase the density at the sonic point, because in this case the density falls off at large distances as a power law, while in the no-wind solution it falls off exponentially. We therefore expect  $\Delta_b > 10$ , and conclude that the condition for isothermality should be valid. Before  $z \sim 4$ , we expect the cooling time to be shorter than the dynamical time by more than an order of magnitude.

#### 4 DISCUSSION

We analyzed the continuous evaporation from dwarf galaxies by thermal winds during the period when an ionizing flux was effective. We found that the critical virial velocity for significant evaporation is significantly higher than computed before assuming an instantaneous mass loss. For example, if the ionization starts at  $z_{ion} = 10$  and is maintained until  $z_{end} = 2$ , a mass loss of one  $e$ -fold occurs in haloes of  $V_{evap} \simeq 24$  to  $34 \text{ km s}^{-1}$ , depending on whether Hydrogen or also Helium are reionized respectively. One  $e$ -fold of gas is lost within the first Hubble time at  $z = 10$  for haloes of  $V_{evap} \simeq 20$  to  $29 \text{ km s}^{-1}$  respectively.

Before we continue with the discussion of possible implications, we should mention the main caveats in our analysis. First, we assumed spherical symmetry for the system of dark halo and gas. This is generally not strictly valid, because the galaxies are typically triaxial configurations which may also involve significant substructure. The fact that the equipotential surfaces tend always to be rounder than the equidensity surfaces helps making the spherical approximation sensible for our analysis. Nevertheless, this is a limitation on the accuracy of our results.

The other caveat, as discussed before, is the fact that the sonic radius obtained is typically comparable to the halo virial radius. On scales larger than the virial radius, one may expect the potential wells to deviate from the NFW profile and be perturbed by neighboring structure. In fact, the potential well need not be spherically symmetric there, nor should it even continue to increase at very large distances. This implies that one should not take too seriously the wind solution at  $r > r_v \sim r_s$ . For example, the formal solution shown in Fig. 1 indicates that the wind continues to accelerate past the sonic point to more than twice the sound speed at large radii. This will not necessarily be the case. Nevertheless, once the wind turns super-sonic, it obviously cannot affect conditions present upstream. This implies that as long

as the sonic point or regions internal to it are not affected by nearby haloes, conditions at the sonic point which determine the mass loss rate, will not change.

As long as the IGM is ionized, accreting gas is not expected to quench the steady thermal winds. This is because the Jeans scale corresponds to haloes of virial velocity  $\sim 30 \text{ km s}^{-1}$  or larger (e.g. Barkana & Loeb 2001), implying that no significant gas infall is expected into haloes that support a steady wind.

The upper critical velocity for evaporation is thus comparable to the Jeans scale, and significantly larger than the cooling barrier at  $\sim 10 \text{ km s}^{-1}$ , below which it is believed that luminous galaxies cannot form. This implies that every halo in the crude range  $10 - 30 \text{ km s}^{-1}$  is likely to be affected by the photo-evaporation process. The mass fraction in such haloes is on the order of 5% at any given time after  $z \sim 10$ . Some of them eventually merge into bigger haloes, but some end up as dwarf haloes today. Among these unmerged haloes, those that managed to form some stars prior to  $z_{ion}$  possibly make low-surface-brightness dwarf galaxies which are dominated by an old population of stars and with no original gas retained. Young stars can form from newly accreted gas after the ionization stops. These objects may resemble the dwarf spheroidals of the Local Group. The other haloes in the range  $10 - 30 \text{ km s}^{-1}$ , those that are dynamically younger and did not form stars prior to  $z_{ion}$ , were doomed to never form stars, at least until  $z_{end}$ . They are likely to end up as completely dark haloes. These are therefore not limited to the mini haloes below the cooling barrier of  $\sim 10 \text{ km s}^{-1}$ , but they rather extend up to  $\sim 20 - 30 \text{ km s}^{-1}$ . This may help explain the apparent discrepancy between the predicted mass function and the observed luminosity function at the faint end. While certain variants of the currently accepted cosmological model may predict a number density for subhalo satellites in big haloes that matches the observed population of Local-Group dwarf galaxies in the range  $V > 20 - 30 \text{ km s}^{-1}$ , it is much harder for such models to recover the small number at  $V < 20 \text{ km s}^{-1}$  (Zetner & Bullock 2003). This can be explained by the very efficient photo-evaporation of gas taking place in haloes below  $V_{evap} \sim 20 \text{ km s}^{-1}$ , as found by our wind analysis.

Given our results, we may attempt to address additional aspects of the possible scenario for dwarf spheroidal galaxies. They are constrained to form in haloes which lie in the crude range  $10 \leq V \leq 30 \text{ km s}^{-1}$ . The gas in haloes of  $V < 10 \text{ km s}^{-1}$  cannot cool to form stars at any early epoch because the cooling rate has a sharp drop below  $T \simeq 10^4 \text{ K}$ ; any molecular hydrogen that is necessary for cooling at  $T < 10^4 \text{ K}$  is likely to be dissociated even before reionization. Efficient cooling by Hydrogen recombination at  $T \gtrsim 10^4 \text{ K}$  can lead to an early burst of stars in haloes of  $V \gtrsim 10 \text{ km s}^{-1}$ . The associated supernovae blow out part of the gas, as they do with a gradually decreasing efficiency in all haloes of  $V < 100 \text{ km s}^{-1}$  (Dekel & Silk 1986; Dekel & Woo 2003). In  $V < 30 \text{ km s}^{-1}$  haloes, the rest of the gas photo-evaporates in a few Hubble times, as computed above. No further gas can fall in as long as the ionizing flux is effective, which may last until  $z \sim 1 - 2$ . This leads to a gas-poor, old-population stellar system. Any recent star formation in these dwarf spheroidals must be due to gas falling in after the ionizing flux became ineffective.

An inspection of the global properties of dwarf galaxies indicates that the dwarfs in the range  $10 - 30 \text{ km s}^{-1}$  span more than two orders of magnitude in luminosity, or stellar mass  $M_*$  (Dekel & Woo 2003). They show no significant correlation between velocity and luminosity, contrary to the irregular, disk dwarf galaxies that are typically larger than  $\sim 30 \text{ km s}^{-1}$  and tend to lie on an extension of the tight Tully-Fisher relation defined by the brighter galaxies. This observed property is consistent with the scenario sketched above for the dwarf spheroidals. The spread in  $M_*$  within this family represents variations in quantities other than halo velocity, such as the proximity of the earlier star formation epoch to  $z_{\text{ion}}$ . The spread in  $M_*$  for a given halo  $V$  becomes much smaller for the larger dwarf irregulars and bright galaxies because haloes above  $V_{\text{evap}}$  retain a larger fraction of their gas and being above the Jeans scale they allow further accretion of more gas. Star formation is thus allowed to occur in these objects also after  $z_{\text{ion}}$ , such that a large fraction of the remaining gas can turn into stars. This brings the value of  $M_*$  close to the value predicted by the energy requirement for gas removal by supernova, which is a strong function of the halo virial velocity:  $M_*/M \propto V^2$  (Dekel & Woo 2003).

The above scenario may also explain why the dwarfs at the low end,  $10 - 30 \text{ km s}^{-1}$ , are typically spheroidals with low spin, while the larger dwarfs tend to be disks. According to the above scenario, the stars in the smaller galaxies are made from the gas that cooled first, namely the gas residing in the inner halo. This gas is typically of specific angular momentum significantly lower than the average for that halo (Bullock *et al.* 2001b; Maller & Dekel 2002). In fact, the scenario predicts a correlation between  $M_*$  and stellar spin parameter because the low- $M_*$  dwarfs typically form later, closer to  $z_{\text{ion}}$ . The smaller fraction of gas involved in the fainter dwarfs must have originated from inner halo regions which host the low-end tail of the specific angular-momentum distribution. There is a hint for such a correlation in the Local Group dwarf spheroidals (Dekel & Woo 2003).

The photo-evaporation process discussed in this paper may involve a non-negligible fraction of the gas in the universe. If it evaporated from dwarfs after they formed stars, it could carry metals with it and enrich the IGM. This could provide a lower limit to the actual enrichment, which is probably dominated by supernova blowout. We estimated for the standard  $\Lambda$ CDM cosmology that at any given time about 5% of the mass is in haloes that can allow significant evaporation. Integrated over time, we find that by  $z \sim 1$  about 40% of the mass is in haloes of  $V > 10 \text{ km s}^{-1}$ . A significant fraction of this mass must have been in haloes in the evaporating range for more than a dynamical time sometime during the merger history. This implies that up to 40% of the gas has been evaporated from dwarf galaxies, and could carry metals.

## ACKNOWLEDGMENTS

This research has been supported by the Israel Science Foundation grants 201/02 and 213/02, by the German-Israel Science Foundation grant I-629-62.14/1999, and by NASA ATP grant NAG5-8218.

## REFERENCES

- Babul A., Rees M.J., 1992, MNRAS, 255, 346  
 Bardeen J.M., Bond J.R., Kaiser N., Szalay A.S., 1986, ApJ, 304, 15  
 Barkana R., Loeb A., 1999, ApJ, 523, 54  
 Barkana R., Loeb A., 2001, PhR, 349, 125  
 Brandt J.C., 1970, Introduction to the solar wind, Series of Books in Astronomy and Astrophysics, Freeman, San Francisco  
 Bryan G., Norman M., 1998, ApJ, 495, 80  
 Bullock J.S., Kolatt T.S., Sigad Y., Somerville R.S., Kravtsov A.V., Klypin A.A., Primack J.R., Dekel A., 2001a, MNRAS, 321, 559  
 Bullock J.S., Dekel A., Kolatt T.S., Kravtsov A.V., Klypin A.A., Porciani, C., Primack J.R., 2001b, ApJ, 555, 240  
 Carroll S.M., Press W.H., Turner E.L., 1992, ARA&A, 30, 499  
 Dekel A., Silk J., 1986, ApJ, 303, 39  
 Dekel A., Woo J., 2003, submitted (astro-ph/0210454)  
 Haiman Z., Rees M.J., Loeb A., 1996, ApJ, 467, 522  
 Katz N., Weinberg D.H., Hernquist L., 1996, ApJS, 105, 19  
 Kepner J.V., Babul A., Spergel D.N., 1997, ApJ, 487, 61  
 Lamers H.J.G.L.M., Cassinelli, J.P., 1999, Introduction to stellar winds, Cambridge University Press  
 Loeb A., Barkana R., 2001, ARA&A, 39, 19  
 Maller A.H., Dekel A., 2002, MNRAS, 335, 487  
 Mateo M., 1998, ARA&A, 36, 435  
 Miralda-Escude J., Rees, M.J., 1998, ApJ, 497, 21  
 Miralda-Escud J., 2000, ApJ, 528, L1  
 Navarro J.F., Frenk C.S., White S.D.M., 1996, ApJ, 462, 563  
 Parker E.N., 1960, ApJ, 132, 821  
 Press W.H., Schechter P., 1974, ApJ, 187, 425  
 Sheth R.K., Tornem G., 1999, MNRAS, 308, 119  
 Sutherland R., Dopita M., 1993, ApJS, 88, 253  
 Woo J., Dekel A., 2003, in preparation  
 Zentner A.R., Bullock J.S., 2003, ApJ, submitted (astro-ph/0304292)